Author Response:

We thank these reviewers for their very helpful comments and suggestions.

Comments from Referee #1

This paper discusses the composition and the oxidation state of sulfur in atmospheric aerosols collected in the general Atlanta area. The overall work is of interest to the community and is well written and has adequate discussion regarding the basic results. Some better presentation of the data and results and clarification of data processing methods however, should be included in at least the supplemental materials.

Specific Comments:

page 5, line 15: I very much like the addition of the sulfate standard database in the supplemental material. However, can the authors address the potential of self-absorption effects of sulfate standards? Particularly as this may possibly contribute to broadness and amplitude reduction of some of the standard peaks? Can the authors elaborate more on whether these data were collected in the bulk or microscale mode? Any more info on the standards particle size, more than "homogenized"?

Sulfur standards were ground using an agate mortar and pestle to the consistency of a fine talcum powder (approximately 10 microns). A cellulose acetate filter was gently dredged through a small quantity (less than 1 mg) of powder placed on a microscope slide. This procedure produced a thin and almost imperceptible coating on the filter in order to limit the thickness and thus self-absorption. S-NEXFS spectra of sulfate standards were collected in bulk mode. Self-absorption must be carefully controlled when measuring fluorescent X-rays from thick specimens; however, the effects of self-absorption are limited to the region of the spectrum above the K-edge (Iida and Noma, 1993; Bajt et al., 1993). In our repeated measurements, the post-edge features were consistent and reproducible which allows us to distinguish between sulfate standards.

This text was added to the Methods section under Sulfate Standards (page 5).

Supplemental material should at least include some plots of NEXFS spectra and their fit results of some typical sample to be able to evaluate the data quality and method of fitting. Both types of fitting with the linear combination of sulfate standards and the use of Gaussian functions should be shown.

Additional figures were added to the supplement that show exemplars of both the linear combination fitting and Gaussian peak fitting that were used to determine the sulfate composition and relative abundance of each oxidation state, respectively.

Figures S1 and S2 were added to pages 4 & 5 of the Supplementary Information.

page 5, line 34: The authors follow a rigorous method of following the monochromator energy drift. However, they do not reference what was mono energy was calibrated with initially? This information is critical to allow comparison to any other published dataset of sulfur spectroscopy.

The energy was calibrated using an elemental sulfur standard (S^0) measured at beamline 2-ID-B. The whiteline energy of the elemental sulfur standard was aligned to 2472 eV (Cozzi et al., 2009). All subsequent data uses 2472 eV as the reference energy for S^0 during the data alignment mentioned by Reviewer 1. Furthermore, for every measurement two spectra are collected: the specimen and an aluminum sulfate standard on the monitor stick. This approach means that all spectra are referenced to the aluminum sulfate standard and the initial calibration is not as crucial on this beamline.

This text was added to the Methods section under Synchrotron-based Spectromicroscopy (page 5-6).

Was there any calibration of the sulfur concentration in the samples? If so, was this a theoretical calculation or an empirical calibration. It would be useful to discuss not only the relative changes in oxidation states, but the overall concentrations observed as well. This information would help in examining the various sources.

The concentrations of sulfur were not measured in this study (see response for next comment below).

Fig S1. I would like to see more information regarding the multiple energy maps. What are the units of the map for each sulfur oxidation state? How were the units determined? Is the intensity here the intensity of the sulfur at each of the white line energies, or was a fit done to calculate the various proportions of each oxidation state? The latter would be a much more rigorous method, as there could be intensity of S0 and SVI is not completely unique to each of the white lines – that is there are contributions of each species to each of the measured energies. A proper method would be to measure the intensities at least N+1 energies (given S0 and SVI, N=2) and do a linear combination fit to determine the N species present at each map pixel. The choice of white line energies compared to the standard library seems off – there white line in the library is at ~2483 eV for sulfate typically, whereas the maps were stated to have been measured at 2480 eV. One would expect, based on the apparent energy calibration, that S0 would appear at 2474 eV. Given the 2480 energy, one may observe some significant intensity of sulfates such as the ammonium sulfates around the energies of S0. Could this mislead the interpretation of S0 in the multiple energy maps if a careful fitting was not performed?

For the multi-energy maps, the units are raw counts from the detector. At this beamline, units such as mass per area are not provided. A more intense signal, that is the more counts present, indicates greater concentrations of sulfur in that region of the sample. The maps were generated at the whiteline energies of S^0 and S^{+VI}. The energies referenced in the methods are the actual settings used during experiment; in other words, these energies are not calibrated with the monitor stick. To identify the correct whiteline energies for the multi-energy mapping, a S-NEXFS spectrum was collected for the particle of interest immediately before mapping. The corresponding whiteline energies for S^0 and S^{+VI} were then taken directly off this spectrum. Individual maps were then collected at the whiteline energies determined for S^0 and S^{+VI}. Although it is possible that the energy drifted during mapping, the interval between the two measurements is short enough that this is not a problem. Due to the 6 eV difference in the whiteline energies of the S^0 and S^{+VI} oxidation states, we do not expect significant overlap between the two oxidation states in multi-energy mapping. Energy drift during mapping may reduce signal intensities of the S^0 and S^{+VI} oxidation states but the overall distribution patterns of the sulfur oxidation states in an individual particle should remain relatively unaffected.

Fitting was not done to determine the relative abundance of sulfur at each oxidation state for each pixel. Instead, more accurate data from individual particle spectroscopy was collected and presented in the paper and supplement.

This text was added to the Methods Section under Synchrotron-based Spectromicroscopy (page 6).

Technical Corrections:

page 5, line33: Did the experiment actually use Vortex SDD with 5 mm^2 area? This seems very small for standard XRF analysis. The more standard value for analysis is 50 mm^2.

The reviewer is correct that the area of the Vortex SSD was 50 mm^2 (page 6).

page 9, line 5: Text refers to Figure S4. This does not exist. Do the authors mean Figure S1?

Text referring to Figure S4 was corrected (page 9).

Comments from Referee #2

General comments:

This paper presents the results of a study on the speciation of sulfur in ambient aerosol samples from the greater Atlanta area. The topic is of interest to this journal and studied with an appropriate technique. The article is generally well written, but the description of data collection and processing needs to be improved before publication.

Specific comments:

Page 3, line 27: Given that secondary sources are discussed for reduced sulfur and the mention of organosulfates in the Discussion section, I think a short sentence on secondary S(+VI) would be warranted.

A short sentence was added to the Discussion about the possibility of secondary formation of sulfates. Using just these techniques, it is unclear what the role of secondary sulfates are in these ambient samples; however, the high concentrations of metal sulfates suggests that secondary processes do influence the composition of S(+VI) in ambient aerosols.

This text was added to the Discussion (page 9).

Page 5, line 13: I commend the inclusion of the standards database in the supplementary information. I do however think that more information on the nature of the measured standards (e.g. particle size) would vastly improve the usefulness of this database.

Sulfur standards were ground using an agate mortar and pestle to the consistency of a fine talcum powder (approximately 10 microns). A cellulose acetate filter was gently dredged through a small quantity (less than 1 mg) of powder placed on a microscope slide. This procedure produced a thin and almost imperceptible coating on the filter in order to limit the thickness and thus self-absorption.

This text has been added to the manuscript in the Methods section under Sulfate Standards (page 5).

Page 5, line 29: the description of the settings doesn't add up properly to me. It states that a 50 eV range was scanned in 0.33 eV steps with a dwell time of 1 s per step. If three full spectra were collected per particle or area (which is how I'd interpret the following sentence), how can the total dwell time be only 3 s? Also, given that multiple spectra were collected for each particle, did you observe any indication of beam damage (especially for S(0))?

Dwell time is used to refer to the time spent at each step in the S-NEXFS spectrum. In this case, because three spectra with a 1 s dwell time each were often necessary to get enough signal for a high quality spectrum, the effective dwell time was at least 3 s because a minimum of 3 s were spent at each energy step in the spectrum. With the 50 eV range and 0.33 eV step-size used in this study, measurements were taken at 150 energies per scan. For 150 energy steps with an effective dwell time of 3 s, the total time required to generate a S-NEXFS spectrum was approximately 7.5 minutes. We did oxidation tests on samples where we measured the same particle repeatedly, creating effective dwell times of more than 10 s. Even with this longer dwell time per energy step, we saw no noticeable shift in oxidation state or the relative abundance of the oxidation states.

Dwell time was defined in the manuscript in the Methods under Synchrotron-based Spectromicroscopy (page 5-6).

Page 5, line 34: It is stated how a potential drift in energy calibration could be monitored. However, no mention is made of the original method of energy calibration. Was a sulfur standard used and if so, which one?

The energy was calibrated using an elemental sulfur standard (S0) measured at beamline 2-ID-B. The whiteline energy of the elemental sulfur standard was aligned to 2472 eV (Cozzi et al., 2009). All subsequent data uses 2472 eV as the reference energy for S0 during the data alignment mentioned by both reviewers. Furthermore, for every measurement two spectra are collected: the specimen and an aluminum sulfate standard on the monitor stick. This approach means that all spectra are referenced to the aluminum sulfate standard and the initial calibration is not as crucial on this beamline.

This text was added to the Methods section under Synchrotron-based Spectromicroscopy (page 5-6).

Page 6, line 31: Some spectra and the associated fits should be shown so that readers are able to evaluate data and fit quality (if nor here, then at least in the Supplementary Information).

Figures were added to the supplement that show exemplars of both the linear combination fitting and Gaussian peak fitting that were used to determine the sulfate composition and relative abundance of each oxidation state, respectively.

Figures S1 and S2 were added to pages 4 & 5 of the Supplementary Information.

Page 6, line 34: The primary emission samples were only characterized at the bulk level. Given that most of the S(0) in the ambient samples was observed only for individual particles, wouldn't this lead to wrong conclusions regarding their comparability?

Reviewer 2 also wanted clarification on the use of bulk emission source data. Emission sources were only characterized at the bulk level, and this poses a problem for data interpretation. We still use the emission source data for comparison with bulk ambient aerosol data and to a limited extent the individual particle data to glean any possible insights; however, we will further clarify that emission sources were collected in the bulk mode and any comparisons between the bulk emission source data and the ambient aerosol individual particle data are speculative.

Text reflecting that the emissions were collected in only bulk mode was added to the Discussion (page 9-10).

Page 8, line 22: This sounds as if this study comes to the conclusion that organosulfates were not present. However, as far as I can see no organosulfate standard was measured, nor are there any comparisons to literature data, so how do the authors come to this conclusion?

In this manuscript, we postulate that organosulfates are not a major component of sulfate aerosol. We were able to account for the sulfate using our present database, which suggests that organosulfates likely do not account for a significant portion of the sulfate aerosol. We do, however, state that contributions near or below 10% could be below the detection limit of this method. Since this is approximately the level that organosulfates are hypothesized to occur, it makes sense that we are able to account for all sulfate present in the sample with our database, even if some small portion of organosulfate is present.

This text was added to the Discussion (page 9).

Table S1: It is clear from this table that measurements of individual particles were only taken for few of the collected samples, in particular at Fire Station 8. Is there any specific reason for that?

Individual particle spectroscopy was not collected for every sample in our collection. Individual particles were examined on samples other than those noted in Table S1; however, the particles did not generate useable spectra. Table S1 represents the number of spectra that were collected that could be used for further analysis.

Text indicating that the number of usable spectra are reflected in Table S1 was added to the Methods Section under Synchrotron-based Spectromicroscopy (page 5).

More information on the generation of the sulfur maps is needed, either in the Data Analysis section or at least in the caption of figure S1. For example: are the maps normalized? What is the unit of the scale bars?

Reviewer 2 also wanted more detailed information to assist with the interpretation of the multi-energy maps presented in Figure S1. For the multi-energy maps, the units are raw counts from the detector. At this beamline, units such as mass per area are not provided. A more intense signal, that is the more counts present, indicates greater concentrations of sulfur in that region of the sample. The maps were generated at the whiteline energies of S0 and S+VI. The energies referenced in the methods are the actual settings used during experiment; in other words, these energies are not calibrated with the monitor stick. To identify the correct whiteline energies for the multi-energy mapping, a S-NEXFS spectrum was collected for the particle of interest immediately before mapping. The corresponding whiteline energies for S0 and S+VI were then taken directly off this spectrum. Individual maps were then collected at the whiteline energies determined for S0 and S+VI. Although it is possible that the energy drifted during mapping, the interval between the two measurements is short enough that this is not a problem. Due to the 6 ev difference in the whiteline energies of the S0 and S+VI oxidation states, we do not expect significant overlap between the two oxidation states in multi-energy mapping. Energy drift during mapping may reduce signal intensities of the S0 and S+VI oxidation states but the overall distribution patterns of the sulfur oxidation states in an individual particle should remain relatively unaffected.

Fitting was not done to determine the relative abundance of sulfur at each oxidation state for each pixel. Instead, more accurate data from individual particle spectroscopy was collected and presented in the paper and supplement.

This text was added to the Methods Section under Synchrotron-based Spectromicroscopy (page 6).

Technical corrections:

page 5, line 35: "monochrometer" should be "monochromator”

This was addressed (page 6).

page 6, line 8: “raster” should be “rastered”

This was addressed (page 6).

Composition and oxidation state of sulfur in atmospheric particulate matter

Amelia F. Longo[1], David J. Vine[2], Laura E. King[1], Michelle Oakes[3], Rodney J. Weber[1], L. G. Huey[1], Armistead G. Russell[1], Ellery D. Ingall[1]

[1]School of Earth and Atmospheric Sciences, Georgia Institute of Technology, 311 Ferst Drive, Atlanta, GA 30332-0340, USA
[2]Advanced Photon Source, Argonne National Laboratory, 9700 S. Cass Avenue, Argonne, IL 60439, USA
[3]Tennessee Department of Environment and Conservation, Division of Air Pollution Control, Nashville, TN 37206, USA

Correspondence to: Ellery Ingall (ingall@eas.gatech.edu)

Abstract. The chemical and physical speciation of atmospheric sulfur was investigated in ambient aerosol samples using a combination of Sulfur Near-Edge X-ray Fluorescence Spectroscopy (S-NEXFS) and X-ray fluorescence (XRF) microscopy. These techniques were used to determine the composition and oxidation state of sulfur in common primary emission sources and ambient particulate matter collected from the greater Atlanta area. Ambient particulate matter samples contained two oxidation states: S^0 and S^{+VI}. Ninety-five percent of the individual aerosol particles (> 1 µm) analyzed contain S^0. Linear combination fitting revealed that S^{+VI} in ambient aerosol was dominated by ammonium sulfate as well as metal sulfates. The finding of metal sulfates provides further evidence for acidic reactions that solubilize metals, such as iron, during atmospheric transport. Emission sources, including biomass burning, coal fly ash, gasoline, diesel, volcanic ash, and aerosolized Atlanta soil, and the commercially available bacterium *Bacillus subtilis*, contained only S^{+VI}. A commercially available *Azotobacter vinelandii* sample contained approximately equal proportions of S^0 and S^{+VI}. S^0 in individual aerosol particles most likely originates from primary emission sources, such as aerosolized bacteria or incomplete combustion.

Formatted: Superscript

Deleted: contain S0 in 95%

Formatted: Superscript

Deleted: Individual particles (> 1 µm)

Formatted: Superscript

Formatted: Superscript

Formatted: Font: Italic

Formatted: Superscript

Formatted: Font: Italic

Formatted: Superscript

Formatted: Superscript

Formatted: Superscript

1 Introduction

Sulfur (S) in atmospheric aerosols has garnered significant interest because of its influence on environmental processes (Bufalini, 1971;Galloway, 1995;Van Grieken et al., 1998) and human health (Burnett et al., 1995). S-rich aerosol can serve as cloud condensation nuclei. On a global scale, cloud condensation nuclei participate in cloud formation processes to change atmospheric albedo (Charlson et al., 1987;Quinn and Bates, 2011), which can ultimately influence global climate. Atmospheric sulfur is responsible for the production of sulfuric acid, which has been implicated in the solubilization of metals in aerosol (Wiederhold et al., 2006;Nenes et al., 2011;Sullivan et al., 2007;Oakes et al., 2012a). Solubilization of recalcitrant mineral phases during atmospheric transport can release nutrient elements, such as iron, which impacts biological productivity in many ocean regions (Longo et al., 2016;Longo et al., 2014;Mahowald et al., 2005;Jickells et al., 2005). Additionally, soluble metals present in the urban environment may cause adverse respiratory events among affected populations (Fang et al., 2016;Pardo et al., 2016).

The range of sulfur oxidation states as well as organic and inorganic forms present in typical samples confound characterization of aerosol sulfur. Characterization approaches including ion chromatography, X-ray fluorescence, and inductively coupled plasma mass spectrometry have been used to quantify bulk elemental or bulk concentrations, which can be used to infer the composition of sulfur in aerosols. However, these techniques cannot determine the oxidation state or directly identify the chemical form of aerosol sulfur. Several studies have demonstrated the effectiveness of synchrotron-based sulfur X-ray absorption near-edge structure (XANES) and the closely related sulfur near-edge X-ray fluorescence spectroscopy (NEXFS) to determine the oxidation state and chemical form of sulfur in environmental samples (Solomon et al., 2003;Prietzel et al., 2011;Morra et al., 1997;Farges et al., 2009); however, the application of these techniques to ambient aerosol samples has largely been limited to studies characterizing a few ambient aerosol samples that aim to explore the feasibility and limits of applying XANES and NEXFS to aerosol sulfur studies (Takahashi et al., 2006;Pongpiachan et al., 2012a;Pongpiachan et al., 2012b;Higashi and Takahashi, 2009;Cozzi et al., 2009).

Deleted:

Consistent with traditional techniques, synchrotron-based XANES studies indicate that sulfur occurs primarily in the S^{+VI} oxidation state, largely, as inorganic sulfate compounds. Primary emission sources of S^{+VI} include both anthropogenic and biogenic sources, including combustion of fossil fuels, biomass burning, volcanoes, and sea spray (Querol et al., 2000). Sulfur in aerosol, ranging in oxidation state from S^{-II} to S^{+IV}, has also been identified in smaller quantities through the use of XANES techniques (Huggins et al., 2000;Eatough et al., 1978;Cao et al., 2015;Higashi and Takahashi, 2009;Craig et al., 1974;Cozzi et al., 2009). Primary sources of reduced sulfur to the atmosphere are mainly attributed to gaseous emissions from volcanic gases, hot springs, bacteria, vehicle exhaust, and oil refineries (Cozzi et al., 2009;Andersson et al., 2006). While detected in the solid phase, reduced sulfur in aerosols has not been extensively studied. Reduced aerosol sulfur may reflect a contribution from primary emission sources or may result from condensation of volatile reduced sulfur gaseous phases, but the ultimate origin of reduced S in aerosol particulates remains unresolved.

Here we use S-NEXFS to investigate the composition and oxidation state of sulfur in ambient aerosols and common primary emission source samples. Previous S-NEXFS studies characterized a limited number of ambient aerosol samples in bulk, providing an average view of the sulfur oxidation state and composition in particulate matter (Higashi and Takahashi, 2009;Takahashi et al., 2006;Pongpiachan et al., 2012a;Pongpiachan et al., 2012b;Long et al., 2014). Recent studies of aerosol iron and selenium have demonstrated that analyzing compositional differences between large particles (> 1 μm) and the bulk sample can help elucidate aerosol sources and transformations (Longo et al., 2016;Oakes et al., 2012b;De Santiago et al., 2014). Following a similar approach, we used a combination of bulk and individual particle S-NEXFS analyses to characterize aerosol sulfur in rural and urban samples and from different emission sources. The spatial distribution of sulfur oxidation states was also characterized in individual particles by mapping particles at different incident energies to gain further insights into the processes surrounding the formation of reduced sulfur species in aerosol.

Deleted: diverse

2 Methods

2.1 Ambient Aerosol Collection

PM2.5 samples were collected from urban and rural locations in and around Atlanta, GA. The five sampling sites, South DeKalb, Fire Station 8, Jefferson Street, Yorkville, and Fort Yargo State Park, are associated with two ongoing studies, the SouthEastern Aerosol Research and Characterization (SEARCH) study (Edgerton et al., 2005;Edgerton et al., 2006;Hansen et al., 2003) and the Assessment of Spatial Aerosol and Composition in Atlanta (Butler et al., 2003). Samples were collected on Zefluor filters over 24-h periods at a flow rate of 16.7 L min^{-1} using cyclone inlet samplers (URG, Chapel Hill, NC). The multichannel particle samplers were mounted approximately 2.5 m off the ground. Three samples were collected from Yorkville (33°55'42.3″N, 85°2'43.68″W), a rural background site for the Atlanta area. Two samples were collected from Jefferson Street (33°46'38.94″N, 84°24'59.58″W), an urban collection site, which is not immediately influenced by any individual source or roadside traffic. Five samples were collected from Fort Yargo State Park (33°58′4.18″N, 83°43′29.16″W), a rural setting that is frequently impacted by biomass burning plumes and power plant emissions. Four samples were collected in South DeKalb, a mixed commercial–residential area, approximately 1 km from a major interstate (33°41′16.48″N, 84°17′25.26″W). Eight samples were collected from Fire Station 8, located in an industrial area within close proximity to a rail yard, a fire station, and an intersection with heavy diesel truck traffic (33°48′6.01″N, 84°26′8.75″W; Table S1).

2.2 Emission Source Collection

PM2.5 samples were collected from gasoline and diesel exhaust, biomass burning, and coal fly ash (Oakes et al., 2012a). Emissions from ultralow sulfur diesel fuel running a 10.8 L engine and conventional gasoline fuel running a 3.3 L engine were collected according to US Environmental Protection Agency protocols under typical urban driving conditions (Liu et al., 2008;Oakes et al., 2012a). Polydisperse coal fly ash, provided by The Southern Co., from an electrostatic precipitator of a midsized coal-fired power plant was aerosolized and collected with a cyclone inlet sampler to separate the PM2.5 fraction (Oakes et al., 2012a). Smoke produced from the burning of materials collected from coniferous and deciduous trees native to Georgia, USA, was sampled during a controlled biomass burning experiment using a cyclone inlet sampler placed 3.5 m above the burn area at a flow rate of 16.7 L min^{-1} for approximately 30 min. The ash produced from the biomass burning experiment was analyzed in the same manner. The above primary emission source samples were collected on polytetrafluoroethylene (Zefluor) filters (Longo et al., 2014). In addition, two commercially available bacteria samples, *Azotobacter vinelandii* (Sigma A2135) and *Bacillus subtilis* (Sigma B4006), were homogenized with agate mortar and pestle and mounted on a cellulose acetate filter for analysis.

All samples were immediately stored after preparation in clean Petri dishes at −20 °C until analysis. Preparation for synchrotron analyses consisted of mounting an approximate 0.5 cm × 0.5 cm section of ambient aerosol and primary emission source filters over a slot on an aluminum support.

2.3 Sulfate Standards

In order to create a database of inorganic sulfate standards necessary for the data analysis described below, ten compounds were analyzed using the same experimental setup and synchrotron system as the ambient aerosols. These standards included, ammonium sulfate (CAS 7783-20-2), barite, copper(II) sulfate (CAS 7758-98-7), gypsum, iron ammonium sulfate (CAS 7783-85-9), iron(III) sulfate (CAS 15244-10-7), jarosite ($KFe^{3+}_3(OH)_6(SO_4)_2$), magnesium sulfate (CAS 7487-88-9), potassium sulfate (CAS 7778-80-5), and sodium sulfate (CAS 7757-82-6). The sulfur standards were ground using an agate mortar and pestle to the consistency of a fine talcum powder (approximately 10 microns). A cellulose acetate filter was then gently dredged through a small quantity (less than 1 mg) of powder placed on a microscope slide. This procedure produced a thin and almost imperceptible coating on the filter in order to limit the thickness and thus self-absorption. S-NEXFS spectra of sulfate standards were collected in bulk mode. Self-absorption must be carefully controlled when measuring fluorescent X-rays from thick specimens; however, the effects of self-absorption are limited to the region of the spectrum above the K-edge (Bajt et al., 1993;Iida and Noma, 1993). In our repeated measurements, the post-edge features were consistent and reproducible which allows us to distinguish between sulfate standards. A database of sulfate standards is provided in the Supporting Material.

Moved down [1]: A database of sulfate standards is provided in the Supporting Material.

Deleted: All standards were homogenized with an agate mortar and pestle and mounted on a cellulose acetate filter for analysis.

Formatted: Font: (Default) Times New Roman, 10 pt

Formatted: Font: (Default) Times New Roman, 10 pt

Moved (insertion) [1]

2.4 Synchrotron-based Spectromicroscopy

Samples were analyzed on the X-ray fluorescence microscope located at beamline 2-ID-B at the Advanced Photon Source, Argonne National Laboratory. The beamline is optimized to examine samples over a 1–4 keV energy range using a focused X-ray beam with a spot size of approximately 60 nm^2 (McNulty et al., 2003). The energy was calibrated using an elemental sulfur standard (S^0). The whiteline energy of the elemental sulfur standard was aligned to 2472 eV (Cozzi et al., 2009). Sulfur near-edge X-ray fluorescence spectroscopy (S-NEXFS) data were collected in two modes that differ based on spatial resolution. In the first mode, individual sulfur-rich particles with a diameter of greater than 1 μm were identified in X-ray fluorescence maps; these particles were then interrogated with micro S-NEXFS. The number of individual particles examined, that provided usable spectra, are provided in Table S1. The individual sulfur-rich particles seen in X-ray fluorescence maps are obvious contributors to the total sample sulfur. However, much of the total sulfur on an aerosol filter can also be contained in particles that are smaller than 1 μm or less sulfur-rich and therefore less apparent in X-ray fluorescence maps. Therefore, in the second mode, large areas of the filters were also examined with an unfocused beam (spot size = 0.25 mm).

Deleted:)

Deleted: with a PM2.5 inlet

In order to maximize the number of samples analyzed in the allotted time, X-ray fluorescence (XRF) maps were created for a subset of samples by rastering the sample through the focused beam in 0.5 µm steps with an incident energy of 2535 eV. At this resolution, individual sulfur-rich particles were clearly discernible. S-NEXFS spectra were scanned over a 50 eV range centered at 2485 eV in 0.33 eV steps, using a 1 s dwell time at each step. Here, dwell time is used to refer to the time spent at each step in the S-NEXFS spectrum or each pixel in an XRF map. Each S-NEXFS measurement for both bulk and individual sulfur-rich particles were repeated at least 3 times in a single location, creating a minimum effective dwell time of 3 s. For these settings, the total scan time would be approximately 7.5 minutes. X-ray spectromicroscopy data were collected using an energy dispersive silicon drift detector (Vortex with a 50 mm^2 sensitive area). A flow of helium was introduced between the X-ray optical hardware and the sample to reduce elastically scattered X-ray background. An in-line monitor stick coated with an aluminum sulfate standard was measured in parallel with each sample in order to identify and correct for any potential drift in monochromator energy calibration that can occur during analyses (de Jonge et al., 2010)), meaning that for every spectral measurement two spectra are collected: the specimen and an aluminum sulfate standard on the monitor stick. Because the energy was calibrated using elemental sulfur S^0, all the data uses 2472 eV as the reference energy for S^0 during the data alignment to the monitor stick. Oxidation tests were also done on a few samples where the same region or particle was measured repeatedly, creating effective dwell times of more than 10 s. Even with this longer dwell time, there was no noticeable shift in oxidation state or the relative abundance of the oxidation states in the tested samples. Clean areas of filter were examined as blanks and showed negligible background signal.

S-NEXFS provides essentially the same information as another commonly cited technique, S-XANES (sulfur X-ray absorption near-edge structure) spectroscopy. The two techniques differ primarily in the method of signal detection. S-NEXFS uses the X-ray fluorescence signal, which is inversely proportional to the absorption signal used in a XANES measurement.

Additionally, XRF microscopy was conducted in two modes. First, to map the distribution of sulfur regardless of oxidation state an incident energy above the S K-edge (2535 eV) was used, and samples were rastered through the focused beam in 0.5 µm steps, as mentioned above. In the second mode, the spatial distribution of S^0 and S^{+VI} oxidation states were quickly mapped by selecting an incident X-ray energy tuned to their specific whiteline energies. Because of the energy drift at this beamline it is important to identify the correct whiteline energies for the multi-energy mapping, so a S-NEXFS spectrum was collected for the particle of interest immediately before mapping. The corresponding whiteline energies for S^0 and S^{+VI} were then taken directly off this spectrum. Individual maps were then collected at the whiteline energies determined for S^0 and S^{+VI}. Although it is possible that the energy drifted during mapping, the interval between the two measurements is short enough that this is not a problem. Due to the 6 eV difference between the whiteline energies of S^0 and S^{+VI}, we do not expect significant overlap between the two oxidation states in multi-energy mapping. Energy drift during mapping may reduce signal intensities of S^0 and S^{+VI}, but the overall distribution patterns of the sulfur oxidation states in the individual particle should remain relatively unaffected. These multi-energy XRF maps were completed in 0.3 µm spatial resolution and 0.5s dwell time per pixel. X-ray focusing was adjusted to maintain a consistent beam spot size

Deleted: s

Deleted: ,

Deleted: zinc

Deleted: e

Deleted: e

Deleted: .

Deleted:

Formatted: Superscript

Deleted: chemical

Deleted: s at 2471 eV and 2480 eV respectively

Formatted: Superscript

Formatted: Superscript

Formatted: Superscript

Formatted: Superscript

Formatted: Superscript

Formatted: Superscript

Formatted: Superscript

Formatted: Superscript

at both energies, however some shift in the final image did occur. The images were aligned using the stack registration function of the Fiji software (Schindelin et al., 2012).

2.5 Data Analysis

S-NEXFS data were normalized to create a relative intensity value of approximately 1 for post edge area of the spectra. The data was also processed using a three-point smoothing algorithm built into the software package Athena to remove high frequency noise (Ravel and Newville, 2005). The relative contribution of each oxidation state can be determined by assuming the entire area under the whiteline peaks is representative of total sulfur, and the area under each whiteline peak represents the relative contribution of each oxidation state (Huffman et al., 1991;Xia et al., 1998). The area under the whiteline peaks was determined using the Gaussian peak fitting function of Athena (Ravel and Newville, 2005) (Figure S1). Because of the relatively low contribution of other sulfur oxidation states, only sulfur species containing S^{+VI} oxidation state could be further characterized via linear combination fitting. Linear combination fitting is an effective tool for the deconvolution of spectra of known mixtures (Longo et al., 2014;Long et al., 2014;Huffman et al., 1991;Solomon et al., 2003;Prietzel et al., 2011). Using Athena software, individual particle and bulk S-NEXFS spectra were fit with previously characterized sulfate standard materials using a linear combination approach to determine both speciation and relative abundance of sulfate phases (Ravel and Newville, 2005) (Figure S2). Athena uses a nonlinear, least squares minimization approach to fit spectra of unknown materials with spectra of standard materials and computes an error term, *R* factor, to quantify the goodness of fit produced by a particular linear combination of standard S-NEXFS spectra. The linear combination of standards that yielded the lowest *R* factor reflects the best fit (Ravel and Newville, 2005).

3 Results

3.1 Oxidation State

Azotobacter vinelandii, *Bacillus subtilis*, gasoline and diesel exhaust, biomass burning, and coal fly ash were only characterized at the bulk level (approximately 0.28 mm^2 filter area). These common primary emission sources, with the exception of one bacteria sample, contained sulfur solely in the S^{+VI} oxidation state. *Azotobacter vinelandii* was the only emission source to contain both oxidized and reduced sulfur, with approximately 44% S^{+VI} and 56% S^0 (Figure 1).

At the bulk level, the oxidation state of sulfur in ambient PM2.5 samples is dominated by S^{+VI}; only two samples from South DeKalb contain S^0 at quantities of less than 10% total sulfur (Figure 2). In contrast, individual particles with aerodynamic diameters of greater than 1 µm consistently contain both S^{+VI} and S^0 (Figure 3). Only one out of twenty-three individual particles analyzed did not contain S^0. At Fire Station 8 and Jefferson Street, the individual particles sampled contain on average 10% S^0. Individual particles from South DeKalb average only 4% S^0. The rural individual particles sampled from Fort Yargo and Yorkville contain on average 5% and 9% S^0, respectively. Multi-energy maps revealed that S^{+VI} was present throughout the aerosol particle. Often the highest concentration of S^{+VI} was in the center of the particle, where the most mass is present (Figure S3). The spatial distribution of S^0 was more varied. In some cases, the S^0 was concentrated in the center of the particle with a less

Deleted:

Deleted: that

Deleted: ed

Deleted: ,

Deleted: 1

prominent ring on the outside of the particle. In other cases, the S^0 was most concentrated in only one area of the particle (Figure S3).

Deleted: 1

3.2 Sulfate Composition

The relative contribution of different sulfur species can be determined by the deconvolution of S-NEXFS spectra with linear combination fitting (Prietzel et al., 2011;Ravel and Newville, 2005). In these samples, only S^{+VI} could be further characterized through linear combination fitting because it was by far the most abundant species of sulfur present in the samples. The regions of the S-NEXFS spectra represented by the lower sulfur oxidation states did not possess sufficient detail to yield compositional information. Because of spectral similarities between various metal sulfates, linear combination fits using copper(II) sulfate or iron(III) sulfate often yielded fits with similar *R* factors. This makes the absolute determination of metal sulfate composition difficult, thus, iron(III) sulfate, copper(II) sulfate, and jarosite are referred to collectively as metal sulfates. The specific compositional information derived from the best linear combination fits, i.e. iron(III) sulfate, copper(II) sulfate, or jarosite, is presented in Tables S2 and S3, and suggests that a combination of iron and copper sulfates are likely present in these samples. In common primary emission sources and ambient PM2.5, S^{+VI} corresponded to sulfate aerosol. In emission sources, only biomass burning, coal fly ash, and diesel exhaust had robust enough signals to characterize specific sulfate composition, and each source had a unique sulfate composition (Table S3). Biomass burning contained potassium sulfate (100 ± 0.005%). Coal fly ash contained gypsum (100 ± 0%), the mineral form of calcium sulfate. Diesel exhaust contains ammonium sulfate (70 ± 11%) and metal sulfate (30 ± 12%).

The composition of sulfate was generally consistent within a sampling location (Table S3 and Figure 4). At the bulk level, rural sampling locations contain a mix of ammonium sulfate and metal sulfate. Yorkville samples are comprised of 61 ± 9% ammonium sulfate and 39 ± 9% metal sulfate, and Fort Yargo samples contain 84 ± 7% ammonium sulfate and 16 ± 7% metal sulfate. Bulk urban samples all contain a large fraction of ammonium sulfate. Samples from Fire Station 8 contain ammonium sulfate (84 ± 7%) mixed with metal sulfate (14 ± 16%), and Jefferson Street contains ammonium sulfate (51 ± 8%) combined with metal sulfate (50 ± 10%). South DeKalb has three different compositional groups at bulk level: (1) ammonium sulfate (63 ± 7%), metal sulfate (29 ± 6%), and potassium sulfate (8 ± 13%); (2) ammonium sulfate (42 ± 14%) and metal sulfate (58 ± 14%); and (3) gypsum (43 ± 15%) and metal sulfate (58 ± 15%).

Only individual particle S-NEXFS spectra from Fire Station 8, Fort Yargo, and South DeKalb contained enough sulfur to determine the sulfate composition (Table S3 and Figure 4). In total, 17 individual particle S-NEXFS spectra were used to gain insights on the sulfate composition of ambient PM2.5. Consistent with the bulk results, individual particles sampled from Fire Station 8 are largely ammonium sulfate and metal sulfate, with the remainder made of gypsum. Individual particles from South DeKalb contain either ammonium sulfate or metal sulfate. Individual particles from Fort Yargo contain a mixture of mostly ammonium sulfate and potassium sulfate with additional contributions from metal sulfate and gypsum. Spectral signals of samples from Jefferson Street and Yorkville were not strong enough to characterize the composition of sulfate in the ambient PM2.5 samples.

4.0 Discussion

Ammonium sulfate and gypsum are commonly identified phases in studies of aerosol sulfate composition (Long et al., 2014;Higashi and Takahashi, 2009;Takahashi et al., 2006). Consistent with these studies, ammonium sulfate was found across all urban and rural sampling locations, and either ammonium sulfate or gypsum were a major constituent of all bulk samples. At the individual particle level, ammonium sulfate was also a primary contributor to sulfate composition; however, potassium and metal sulfates became more apparent. Our results showed that the sulfate in biomass burning was dominated by potassium sulfate, which suggests biomass burning may be the primary source of the potassium sulfate in ambient aerosol samples. Potassium is often used as a tracer for biomass burning in source apportionment studies (Viana et al., 2008), which show that biomass burning can contribute up to 40% of total PM2.5 in Georgia's spring months and 10% of total PM2.5 in Georgia's summer months (Tian et al., 2009). Organosulfates have recently been identified as a significant component of sulfate aerosol (Liao et al., 2015;Schmitt-Kopplin et al., 2010;Surratt et al., 2008;Xu et al., 2015). In this study, organosulfates were not identified as a constituent of sulfate aerosol. While organosulfates are not present in our sulfate standard database, we were able to account for all the sulfate in our samples without this class of compounds. However, the expected concentration of organosulfates in ambient aerosol could be near or below 10%, the detection limit of linear combination fitting techniques (Longo et al., 2014;Oakes et al., 2012a;Oakes et al., 2012b), so organosulfates may still be present in small quantities.

Metal sulfates were identified as a constituent of all the bulk ambient particulate matter samples and 53% of individual particle spectra. Linear combination fitting of S-NEXFS spectra suggests that iron(III) sulfates are an important group of metal sulfates in ambient Atlanta aerosol (Table S2 & S3). Furthermore, an Fe-XANES study of ambient Atlanta particulate matter identified iron(III) sulfates, which accounted for approximately 20% of the total iron (Oakes et al., 2012a). Iron sulfate represent a very soluble, bioavailable, form of iron that has been found in ambient aerosol (Zhang et al., 2014;Moffet et al., 2012;Schroth et al., 2009;Oakes et al., 2012a). Diesel exhaust was the only primary emission source to contain metal sulfates in this study, and because source apportionment studies show that diesel emissions accounts for approximately 5.3% of PM2.5 in Atlanta (Hu et al., 2014), it is unlikely that diesel exhaust alone can explain the quantities of metal sulfates found in our ambient aerosol samples. This could suggest that secondary processes play a role in the composition of S^{+VI} in ambient aerosol samples. Iron sulfate may be the end product of acidic reactions hypothesized to occur in the atmosphere that are responsible for solubilizing iron. Correlations between the sulfur content and iron solubility have previously been used to suggest this mechanism plays a role in shaping the composition of iron in ambient Atlanta aerosol (Oakes et al., 2012a). Briefly, sulfuric acid solubilizes more crystalline iron phases resulting in a solution rich in soluble iron and sulfate that can become internally mixed and potentially precipitate out as iron(III) sulfate (Moffet et al., 2012;Zhang et al., 2014;Oakes et al., 2012a). Evidence of similar processes has been found for copper (Fang et al., 2015), which is another metal that is likely present in these samples (Table S2 and Table S3). The metal sulfates seen in ambient Atlanta aerosol are likely the product of both primary emission sources as well as secondary reactions.

In the multi-energy maps, S^0 always occurs with S^{+VI} (Figure S3), suggesting they are either co-emitted as a primary source or linked by a secondary formation process that occurs in the atmosphere. Up to 20% of the sulfur in individual particles was in the reduced form, as S^0. Previous examinations of ambient aerosol have reported less than

Deleted: ;

Deleted: h

Deleted:

Deleted: s

Deleted: are

Deleted: expected to occur at

Deleted: NEXFS and

Deleted: can

Formatted: Superscript

Deleted: also

Deleted: acidic

Deleted: 4

5% of total sulfur as reduced sulfur (Cozzi et al., 2009;Long et al., 2014) and have suggested incomplete combustion or incinerator emissions as the likely source (Andersson et al., 2006;Bao et al., 2009;Matsumoto et al., 2006). Common primary emission sources, such as gasoline and diesel exhaust, coal fly ash, and biomass burning, did not contain S^0 as a readily identifiable constituent in bulk S-NEXFS spectra, leaving the source of reduced S in ambient Atlanta aerosol unresolved. While emission sources were not analyzed at the individual particle level, bulk S-NEXFS of *Azotobacter vinelandii* revealed this bacterium to be the only analyzed emission source to be enriched in S^0. Microbial cells are increasingly recognized as an important natural component of aerosol (Burrows et al., 2009;Bauer et al., 2002). The ubiquitous distribution of bacteria makes aerosolized soil bacteria, such as *Azotobacter vinelandii*, another potential primary source of S^0. Furthermore, S^0 was commonly found in individual particles, which constitute the largest particle size fraction of these samples (>1 µm). This could further support the hypothesis that the S^0 is from aerosolized soil bacteria, which would reside in larger particles.

Deleted: Here

Deleted: to be the only analyzed potential

The reduced sulfur found in ambient aerosol particles could also be a result of secondary formation processes that occur in the atmosphere. In a previous study, S^{+IV} found in ambient particle matter was attributed to the absorption and incorporation of sulfur dioxide (S^{+IV}) onto atmospheric particulate matter (Higashi and Takahashi, 2009). Theoretically, a similar mechanism could help explain the finding of S^0 in ambient aerosols, however, gaseous phases of reduced sulfur compounds are unlikely to absorb onto an aerosol surface or condense without undergoing oxidation (Alexander et al., 2005;Liao et al., 2003). Furthermore, reduced sulfur species on the surface of a particle would be easily oxidized by ozone, oxygen, or the hydroxyl radical, suggesting that only reduced sulfur inside of a heterogeneous particle would be likely to survive (Long et al., 2014), suggesting that the S^0 likely has a primary source.

The composition and oxidation state of sulfur in ambient aerosol provide insights for atmospheric chemistry involving sulfur as well as metals. More than 25% of the bulk sulfate composition can be attributed to metal sulfates, which cannot be accounted for by our primary sources alone (Hu et al., 2014). The solubilization of metals with sulfuric acid during atmospheric transport likely plays a role in the forming the metal sulfates observed in this study as well as others (Oakes et al., 2012a). Reduced sulfur was also found to account for up to 20% of the total sulfur in individual particles, which is a higher fraction than typically observed in ambient aerosol samples (Long et al., 2014;Cozzi et al., 2009). As is the case with previous studies that have noted reduced sulfur in ambient aerosol samples, the S^0 is likely from a primary emission source. Incomplete combustion is the most commonly cited source of reduced sulfur compounds found in aerosol (Long et al., 2014;Cozzi et al., 2009;Bao et al., 2009;Matsumoto et al., 2006;Andersson et al., 2006); however, in this study, a bacterium was the only potential primary emission source to contain S^0 at the bulk level. This suggests that aerosolized bacteria may contribute to the S^0 seen in ambient Atlanta aerosol.

Deleted: s

Deleted: the

References

Alexander, B., Park, R. J., Jacob, D. J., Li, Q. B., and Yantosca, R. M.: Sulfate formation in sea-salt aerosols: Constraints from oxygen isotopes, Journal of Geophysical Research, 110, 10.1029/2004JD005659, 2005.

Andersson, J. T., Hegazi, A. H., and Roberz, B.: Polycyclic aromatic sulfur heterocycles as information carriers in environmental studies, Analytical and Bioanalytical Chemistry, 386, 891-905, 10.1007/s00216-006-0704-y, 2006.

Bajt, S., Clark, S. B., Sutton, S. R., Rivers, M. L., and Smith, J. V.: Synchrotron X-ray microprobe determination of chromate content using X-ray-Absorption Near-Edge Structure, Analytical Chemistry, 65, 1800-1804, 10.1021/ac00061a026, 1993.

Bao, L. M., Lin, J., Liu, W., Lu, W. Z., Zhang, G. L., Li, Y., Ma, C. Y., Zhao, Y. D., He, W., and Hu, T. D.: Investigation of sulfur speciation in particles from small coal-burning boiler by XANES spectroscopy, Chinese Physics C, 33, 1001-1005, 2009.

Bauer, H., Kasper-Giebl, A., Loflund, M., Giebl, H., Hitzenberger, R., Zibuschka, F., and Puxbaum, H.: The contribution of bacteria and fungal spores to the organic carbon content of cloud water, precipitation and aerosols, Atmospheric Research, 64, 109-119, 10.1016/s0169-8095(02)00084-4, 2002.

Bufalini, M.: Oxidation of sulfur dioxide in polluted atmospheres - review, Environmental Science & Technology, 5, 685-&, 10.1021/es60055a001, 1971.

Burnett, R. T., Dales, R., Krewski, D., Vincent, R., Dann, T., and Brook, J. R.: Associations between ambient particulate sulfate and admissions to Ontario hospitals for cardiac and respiratory-diseases, American Journal of Epidemiology, 142, 15-22, 1995.

Burrows, S. M., Elbert, W., Lawrence, M. G., and Poschl, U.: Bacteria in the global atmosphere - Part 1: Review and synthesis of literature data for different ecosystems, Atmospheric Chemistry and Physics, 9, 9263-9280, 2009.

Butler, A. J., Andrew, M. S., and Russell, A. G.: Daily sampling of PM2.5 in Atlanta: Results of the first year of the assessment of spatial aerosol composition in Atlanta study, Journal of Geophysical Research-Atmospheres, 108, SOS 3-1–SOS 3-11, 10.1029/2002JD002234, 2003.

Cao, J. J., Li, Y. K., Jiang, T., and Hu, G.: Sulfur-containing particles emitted by concealed sulfide ore deposits: an unknown source of sulfur-containing particles in the atmosphere, Atmospheric Chemistry and Physics, 15, 6959-6969, 10.5194/acp-15-6959-2015, 2015.

Charlson, R. J., Lovelock, J. E., Andreae, M. O., and Warren, S. G.: Oceanic phytoplankton, atmospheric sulfur, cloud albedo and climate, Nature, 326, 655-661, 10.1038/326655a0, 1987.

Cozzi, F., Pellegrini, I., Adami, G., Reisenhofer, E., Bovenzi, M., and Barbieri, P.: Sulphur speciation of PM10 samples by XANES spectroscopy, Central European Journal of Chemistry, 7, 395-401, 10.2478/s11532-009-0052-9, 2009.

Craig, N. L., Harker, A. B., and Novakov, T.: Determination of chemical states of sulfur in ambient pollution aerosols by X-ray photoelectron-spectroscopy, Atmospheric Environment, 8, 15-21, 10.1016/0004-6981(74)90108-5, 1974.

de Jonge, M. D., Paterson, D., McNulty, I., Rau, C., Brandes, J. A., and Ingall, E.: An energy and intensity monitor for X-ray absorption near-edge structure measurements, Nuclear Instruments & Methods in Physics Research Section a-Accelerators Spectrometers Detectors and Associated Equipment, 619, 154-156, 10.1016/j.nima.2010.01.001, 2010.

De Santiago, A., Longo, A. F., Ingall, E. D., Diaz, J. M., King, L. E., Lai, B., Weber, R. J., Russell, A. G., and Oakes, M.: Characterization of selenium in ambient aerosols and primary emission sources, Environmental Science & Technology, 48, 8988-8994, 10.1021/es500379y, 2014.

Eatough, D. J., Major, T., Ryder, J., Hill, M., Mangelson, N. F., Eatough, N. L., Hansen, L. D., Meisenheimer, R. G., and Fischer, J. W.: FORMATION AND STABILITY OF SULFITE SPECIES IN AEROSOLS, Atmospheric Environment, 12, 263-271, 10.1016/0004-6981(78)90206-8, 1978.

Edgerton, E. S., Hartsell, B. E., Saylor, R. D., Jansen, J. J., Hansen, D. A., and Hidy, G. M.: The southeastern aerosol research and characterization study: Part II. Filter-based measurements of fine and coarse particulate matter mass and composition, Journal of the Air & Waste Management Association, 55, 1527-1542, 2005.

Edgerton, E. S., Hartsell, B. E., Saylor, R. D., Jansen, J. J., Hansen, D. A., and Hidy, G. M.: The Southeastern Aerosol Research and Characterization Study, part 3: Continuous measurements of fine particulate matter mass and composition, Journal of the Air & Waste Management Association, 56, 1325-1341, 2006.

Fang, T., Guo, H., Verma, V., Peltier, R. E., and Weber, R. J.: PM2.5 water-soluble elements in the southeastern United States: automated analytical method development, spatiotemporal distributions, source apportionment, and implications for health studies, Atmospheric Chemistry and Physics, 15, 11667-11682, 10.5194/acp-15-11667-2015, 2015.

Fang, T., Verma, V., Bates, J. T., Abrams, J., Klein, M., Strickland, M. J., Sarnat, S. E., Chang, H. H., Mulholland, J. A., Tolbert, P. E., Russell, A. G., and Weber, R. J.: Oxidative potential of ambient water-soluble PM2.5 in the southeastern United States: contrasts in sources and health associations between ascorbic acid (AA) and dithiothreitol (DTT) assays, Atmospheric Chemistry and Physics, 16, 3865-3879, 10.5194/acp-16-3865-2016, 2016.

Farges, F., Keppler, H., Flank, A. M., and Lagarde, P.: Sulfur K-edge XANES study of S sorbed onto volcanic ashes, Journal of Physics: Conference Series, 190, 10.1088/1742-6596/190/1/012177, 2009.

Galloway, J. N.: Acid deposition: Perspectives in time and space, Water Air and Soil Pollution, 85, 15-24, 10.1007/bf00483685, 1995.

Hansen, D. A., Edgerton, E. S., Hartsell, B. E., Jansen, J. J., Kandasamy, N., Hidy, G. M., and Blanchard, C. L.: The southeastern aerosol research and characterization study: Part 1-overview, Journal of the Air & Waste Management Association, 53, 1460-1471, 2003.

Higashi, M., and Takahashi, Y.: Detection of S(IV) Species in Aerosol Particles Using XANES Spectroscopy, Environmental Science & Technology, 43, 7357-7363, 10.1021/es900163y, 2009.

Hu, Y., Balachandran, S., Pachon, J. E., Baek, J., Ivey, C., Holmes, H., Odman, M. T., Mulholland, J. A., and Russell, A. G.: Fine particulate matter source apportionment using a hybrid chemical transport and receptor model approach, Atmospheric Chemistry and Physics, 14, 5415-5431, 10.5194/acp-14-5415-2014, 2014.

Huffman, G. P., Mitra, S., Huggins, F. E., Shah, N., Vaidya, S., and Lu, F. L.: Quantitative-analysis of all major forms of sulfur in coal by X-ray absorption fine-structure spectroscopy, Energy & Fuels, 5, 574-581, 10.1021/ef00028a008, 1991.

Huggins, F. E., Shah, N., Huffman, G. P., and Robertson, J. D.: XAFS spectroscopic characterization of elements in combustion ash and fine particulate matter, Fuel Processing Technology, 65, 203-218, 10.1016/s0378-3820(99)00089-2, 2000.

Iida, A., and Noma, T.: Correction of the self-absorption effect in fluorescence X-ray absorption fine-structure, Japanese Journal of Applied Physics Part 1 - Regular Papers Short Notes & Review Papers, 32, 2899-2902, 10.1143/JJAP.32.2899, 1993.

Jickells, T. D., An, Z. S., Andersen, K. K., Baker, A. R., Bergametti, G., Brooks, N., Cao, J. J., Boyd, P. W., Duce, R. A., Hunter, K. A., Kawahata, H., Kubilay, N., laRoche, J., Liss, P. S., Mahowald, N., Prospero, J. M., Ridgwell, A. J., Tegen, I., and Torres, R.: Global iron connections between desert dust, ocean biogeochemistry, and climate, Science, 308, 67-71, 10.1126/science.1105959, 2005.

Liao, H., Adams, P. J., Chung, S. H., Seinfeld, J. H., Mickley, L. J., and Jacob, D. J.: Interactions between tropospheric chemistry and aerosols in a unified general circulation model, Journal of Geophysical Research, 108, 4001, 10.1029/2001JD001260, 2003.

Liao, J., Froyd, K. D., Murphy, D. M., Keutsch, F. N., Yu, G., Wennberg, P. O., St. Clair, J. M., Crounse, J. D., Wisthaler, A., Mikoviny, T., Jimenez, J. L., Campuzano-Jost, P., Day, D. A., Hu, W., Ryerson, T. B., Pollack, I. B., Peischl, J., Anderson, B. E., Ziemba, L. D., Blake, D. R., Meinardi, S., and Diskin, G.: Airborne measurements of organosulfates over the continental U. S., Journal of Geophysical Research: Atmospheres, 120, 2990-3005, 10.1002/2014JD022378, 2015.

Liu, Z. G., Berg, D. R., and Schauer, J. J.: Effects of a Zeolite-Selective Catalytic Reduction System on Comprehensive Emissions from a Heavy-Duty Diesel Engine, Journal of the Air & Waste Management Association, 58, 1258-1265, 10.3155/1047-3289.58.10.1258, 2008.

Long, S. L., Zeng, J. R., Li, Y., Bao, L. M., Cao, L. L., Liu, K., Xu, L., Lin, J., Liu, W. J., Wang, G. H., Yao, J., Ma, C. Y., and Zhao, Y. D.: Characteristics of secondary inorganic aerosol and sulfate species in size-fractionated aerosol particles in Shanghai, Journal of Environmental Science-China, 26, 1040-1051, 10.1016/S1001-0742(13)60521-5, 2014.

Longo, A. F., Ingall, E. D., Diaz, J. M., Oakes, M., King, L. E., Nenes, A., Mihalopoulos, N., Violaki, K., Avila, A., Benitez-Nelson, C., Brandes, J., McNulty, I., and Vine, D. J.: P-NEXFS analysis of aerosol phosphorus delivered to the Mediterranean Sea, Geophysical Research Letters, 41, 4043-4049, 10.1002/2014GL060555, 2014.

Longo, A. F., Feng, Y., Lai, B., Landing, W. M., Shelley, R. U., Nenes, A., Mihalopoulos, N., Violaki, K., and Ingall, E. D.: Influence of Atmospheric Processes on the Solubility and Composition of Iron in Saharan Dust, Environmental Science & Technology, 50, 6912-6920, 10.1021/acs.est.6b02605, 2016.

Mahowald, N., Baker, A. R., Bergametti, G., Brooks, N., Duce, R. A., Jickells, T. D., Kubilay, N., Prospero, J. M., and Tegen, I.: Atmospheric global dust cycle and iron inputs to the ocean, Global Biogeochemical Cycles, 19, doi:10.1029/2004GB002402, 2005.

Matsumoto, S., Tanaka, Y., Ishii, H., Tanabe, T., Kitajima, Y., and Kawai, J.: Sulfur chemical state analysis of diesel emissions of vehicles using X-ray absorption, Spectrochimica Acta Part B-Atomic Spectroscopy, 61, 991-994, 10.1016/j.sab.2006.06.013, 2006.

McNulty, I., Paterson, D., Arko, J., Erdmann, M., Frigo, S. P., Goetze, K., Ilinski, P., Krapf, N., Mooney, T., Retsch, C. C., Stampfl, A. P. J., Vogt, S., Wang, Y., and Xu, S.: The 2-ID-B intermediate-energy scanning X-ray microscope at the APS, Journal De Physique Iv, 104, 11-15, 10.1051/jp4:200300019, 2003.

Moffet, R. C., Furutani, H., Rodel, T. C., Henn, T. R., Sprau, P. O., Laskin, A., Uematsu, M., and Gilles, M. K.: Iron speciation and mixing in single aerosol particles from Asian continental outflows, Journal of Geophysical Research, 117, 10.1029/2011JD016746, 2012.

Morra, M. J., Fendorf, S. E., and Brown, P. D.: Speciation of sulfur in humic and fulvic acids using X-ray absorption near-edge structure (XANES) spectroscopy, Geochimica Et Cosmochimica Acta, 61, 683-688, 10.1016/S0016-7037(97)00003-3, 1997.

Nenes, A., Krom, M. D., Mihalopoulos, N., Van Cappellen, P., Shi, Z., Bougiatioti, A., Zarmpas, P., and Herut, B.: Atmospheric acidification of mineral aerosols: a source of bioavailable phosphorus for the oceans, Atmospheric Chemistry and Physics, 11, 6265-6272, 10.5194/acp-11-6265-2011, 2011.

Oakes, M., Ingall, E. D., Lai, B., Shafer, M. M., Hays, M. D., Liu, Z. G., Russell, A. G., and Weber, R. J.: Iron Solubility Related to Particle Sulfur Content in Source Emission and Ambient Fine Particles, Environmental Science & Technology, 46, 6637-6644, 10.1021/es300701c, 2012a.

Oakes, M., Weber, R. J., Lai, B., Russell, A., and Ingall, E. D.: Characterization of iron speciation in urban and rural single particles using XANES spectroscopy and micro X-ray fluorescence measurements: investigating the relationship between speciation and fractional iron solubility, Atmospheric Chemistry and Physics, 12, 745-756, 10.5194/acp-12-745-2012, 2012b.

Pardo, M., Porat, Z., Rudich, A., Schauer, J. J., and Rudich, Y.: Repeated exposures to roadside particulate matter extracts suppresses pulmonary defense mechanisms, resulting in lipid and protein oxidative damage, Environmental Pollution, 210, 227-237, 10.1016/j.envpol.2015.12.009, 2016.

Pongpiachan, S., Thumanu, K., Kositanont, C., Schwarzer, K., Prietzel, J., Hirunyatrakul, P., and Kittikoon, I.: Parameters influencing sulfur speciation in environmental samples using sulfur K-edge X-ray absorption near-edge structure, Journal of Analytical Methods in Chemistry, 10.1155/2012/659858, 2012a.

Pongpiachan, S., Thumanu, K., Na Pattalung, W., Hirunyatrakul, P., Kittikoon, I., Fai Ho, K., and Cao, J. J.: Diurnal variation and spatial distribution effects on sulfur speciation in aerosol samples as assessed by X-ray absorption near-edge structuer (XANES), Journal of Analytical Methods in Chemistry, 10.1155/2012/696080, 2012b.

Prietzel, J., Botzaki, A., Tyufekchieva, N., Brettholle, M., Thieme, J., and Klysubun, W.: Sulfur Speciation in Soil by S K-Edge XANES Spectroscopy: Comparison of Spectral Deconvolution and Linear Combination Fitting, Environmental Science & Technology, 45, 2878-2886, 10.1021/es102180a, 2011.

Querol, X., Alastuey, A., Chaves, A., Spiro, B., Plana, F., and Lopez-Soler, A.: Sources of natural and anthropogenic sulphur around the Teruel power station, NE Spain. Inferences from sulphur isotope geochemistry, Atmospheric Environment, 34, 333-345, 10.1016/s1352-2310(99)00188-0, 2000.

Quinn, P. K., and Bates, T. S.: The case against climate regulation via oceanic phytoplankton sulphur emissions, Nature, 480, 51-56, 10.1038/nature10580, 2011.

Ravel, B., and Newville, M.: ATHENA, ARTEMIS, HEPHAESTUS: data analysis for X-ray absorption spectroscopy using IFEFFIT, Journal of Synchrotron Radiation, 12, 537-541, 10.1107/s0909049505012719, 2005.

Schindelin, J., Arganda-Carreras, I., Frise, E., Kaynig, V., Longair, M., Pietzsch, T., Preibisch, S., Rueden, C., Saalfeld, S., Schmid, B., Tinevez, J. Y., White, D. J., Hartenstein, V., Eliceiri, K., Tomancak, P., and Cardona, A.: Fiji: an open-source platform for biological-image analysis, Nature Methods, 9, 676-682, 10.1038/nmeth.2019, 2012.

Schmitt-Kopplin, P., Gelencser, A., Dabek-Zlotorzynska, E., Kiss, G., Hertkorn, N., Harir, M., Hong, Y., and Gebefugi, I.: Analysis of the Unresolved Organic Fraction in Atmospheric Aerosols with Ultrahigh-Resolution Mass Spectrometry and Nuclear Magnetic Resonance Spectroscopy: Organosulfates As Photochemical Smog Constituents, Analytical Chemistry, 82, 8017-8026, 10.1021/ac101444r, 2010.

Schroth, A. W., Crusius, J., Sholkovitz, E. R., and Bostick, B. C.: Iron solubility driven by speciation in dust sources to the ocean, Nat. Geosci., 2, 337-340, 10.1038/ngeo501, 2009.

Solomon, D., Lehmann, J., and Martinez, C. E.: Sulfur K-edge XANES spectroscopy as a tool for understanding sulfur dynamics in soil organic matter, Soil Science Society of America Journal, 67, 1721-1731, 10.2136/sssaj2003.1721, 2003.

Sullivan, R. C., Guazzotti, S. A., Sodeman, D. A., and Prather, K. A.: Direct observations of the atmospheric processing of Asian mineral dust, Atmospheric Chemistry and Physics, 7, 1213-1236, 2007.

Surratt, J. D., Gomez-Gonzalez, Y., Chan, A. W. H., Vermeylen, R., Shahgholi, M., Kleindienst, T. E., Edney, E. O., Offenberg, J. H., Lewandowski, M., Jaoui, M., Maenhaut, W., Claeys, M., Flagan, R. C., and Seinfeld, J. H.: Organosulfate formation in biogenic secondary organic aerosol, Journal of Physical Chemistry A, 112, 8345-8378, 10.1021/jp802310p, 2008.

Takahashi, Y., Kanai, Y., Kamioka, H., Ohta, A., Maruyama, H., Song, Z., and Shimizu, H.: Speciation of sulfate in size-fractionated aerosol particles using sulfur K-edge X-ray absorption near-edge structure, Environmental Science & Technology, 40, 5052-5057, 10.1021/es060497y, 2006.

Tian, D., Hu, Y. T., Wang, Y. H., Boylan, J. W., Zheng, M., and Russell, A. G.: Assessment of biomass burning emissions and their impacts on urban and regional PM2.5: A Georgia case study, Environmental Science & Technology, 43, 299-305, 10.1021/es801827s, 2009.

Van Grieken, R., Delalieux, F., and Gysels, K.: Cultural heritage and the environment, Pure and Applied Chemistry, 70, 2327-2331, 10.1351/pac199870122327, 1998.

Viana, M., Kuhlbusch, T. A. J., Querol, X., Alastuey, A., Harrison, R. M., Hopke, P. K., Winiwarter, W., Vallius, A., Szidat, S., Prevot, A. S. H., Hueglin, C., Bloemen, H., Wahlin, P., Vecchi, R., Miranda, A. I., Kasper-Giebl, A., Maenhaut, W., and Hitzenberger, R.: Source apportionment of particulate matter in Europe: A review of methods and results, Journal of Aerosol Science, 39, 827-849, 10.1016/j.jaerosci.2008.05.007, 2008.

Wiederhold, J. G., Kraemer, S. M., Teutsch, N., Borer, P. M., Halliday, A. N., and Kretzschmar, R.: Iron isotope fractionation during proton-promoted, ligand-controlled, and reductive dissolution of goethite, Environmental Science & Technology, 40, 3787-3793, 10.1021/es052228y, 2006.

Xia, K., Weesner, F., Bleam, W. F., Bloom, P. R., Skyllberg, U. L., and Helmke, P. A.: XANES studies of oxidation states of sulfur in aquatic and soil humic substances, Soil Science Society of America Journal, 62, 1240-1246, 1998.

Xu, L., Guo, H., Boyd, C. M., Klein, M., Bougiatioti, A., Cerully, K. M., Hite, J. R., Isaacman-VanWertz, G., Kreisberg, N. M., Knote, C., Olson, K., Koss, A., Goldstein, A. H., Hering, S. V., de Gouw, J., Baumann, K., Lee, S., Nenes, A., Weber, R. J., and Ng, N. L.: Effects of anthropogenic emissions on aerosol formation from isoprene and monoterpenes in the southeastern United States, Proceedings of the National Academy of Sciences of the United States of America, 112, 37-42, 10.1073/pnas.1417609112, 2015.

Zhang, G. H., Bi, X. H., Lou, S. R., Li, L., Wang, H. L., Wang, X. M., Zhou, Z., Sheng, G., Fu, J. M., and Chen, C. H.: Source and mixing state of iron-containing particles in Shanghai by individual particle analysis, Chemosphere, 95, 9-16, 10.1016/j.chemosphere.2013.04.046, 2014.

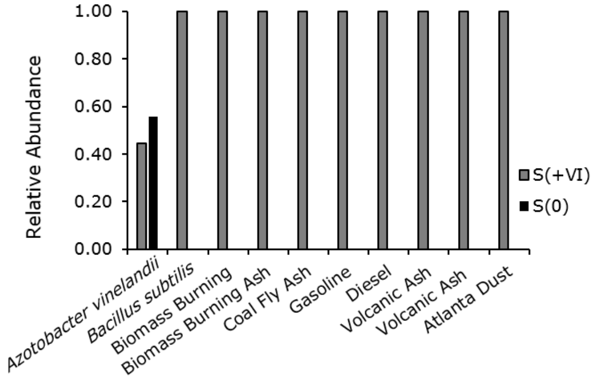

Figure 1: Oxidation state of sulfur in common emission sources Common emission sources were generally dominated by S^{+VI} (grey). Only the bacteria sample *Azotobacter vinelandii* showed a signal for S^{0} as well as S^{+VI}.

5

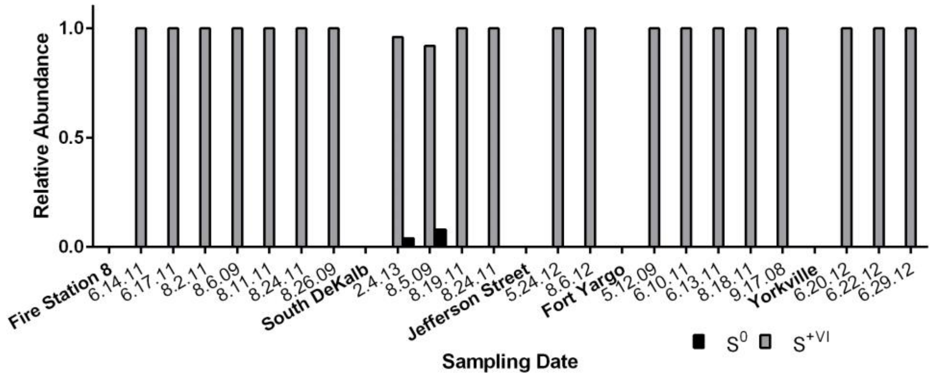

Figure 2: Bulk oxidation state of ambient particulate matter samples Ambient particulate matter samples were characterized at the bulk level for oxidation state. Here, the fractional relative abundance of S^0 (black) and S^{+VI} (grey) are shown for each of the ambient particulate matter samples. S^0 is only present in two samples collected from South DeKalb. The remaining samples contain only S^{+VI} when examined in bulk.

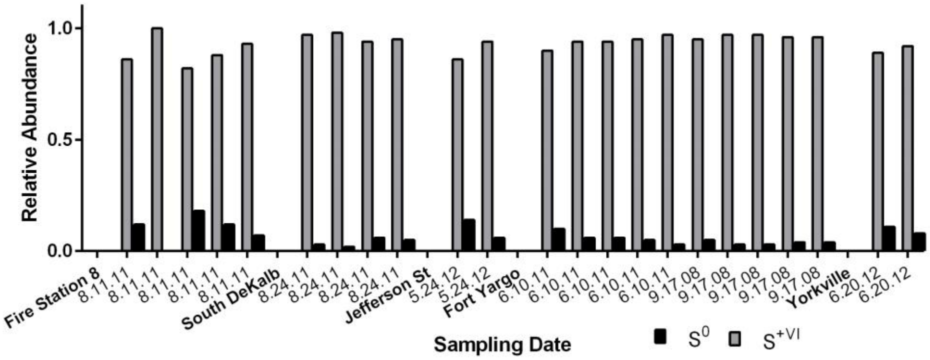

Figure 3: Oxidation state of individual aerosol particles The oxidation state of sulfur was examined in individual particles from a subset of samples. The fractional relative abundance of S^0 (black) and S^{+VI} (grey) is shown for each particle interrogated with S-NEXFS. At the individual particle level, sulfur is consistently seen at both the S^0 and S^{+VI} oxidation states.

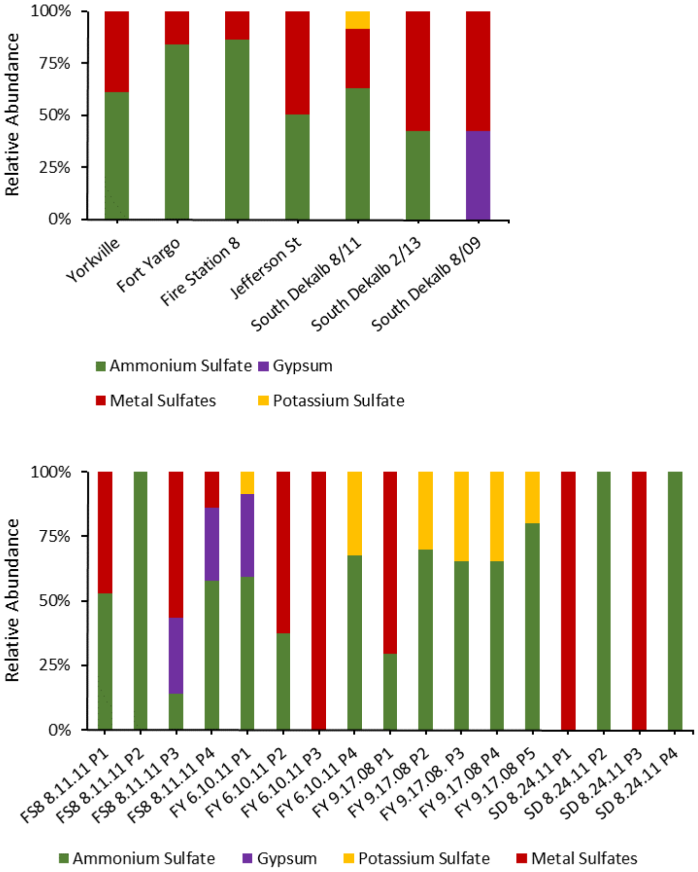

Figure 4: Composition of aerosol sulfate Bulk (top) and individual particle (bottom) composition of sulfur in ambient particulate matter. For bulk samples, the composition of sulfate was consistent for all samples within a particular sampling location, with the exception of South DeKalb. These samples had three different compositional groups, and the month and year of collection are provided next to the samples. For individual particles, the sulfate composition was able to be determined for samples from Fire Station 8 (FS8), Fort Yargo (FY), and South DeKalb (SD). Different particles from the same samples are numbered sequentially (P1-P5).

Supplementary Information for:

Composition and oxidation state of sulfur in atmospheric particulate matter

Amelia F. Longo[1], David J. Vine[2], Laura E. King[1], Michelle Oakes[3], Rodney J. Weber[1], L. Gregory Huey[1], Armistead G. Russell[1], Ellery D. Ingall[1]

[1]School of Earth and Atmospheric Sciences, Georgia Institute of Technology, 311 Ferst Drive, Atlanta, GA 30332-0340, USA
[2]Advanced Photon Source, Argonne National Laboratory, 9700 S. Cass Avenue, Argonne, IL 60439, USA
[3]Tennessee Department of Environment and Conservation, Division of Air Pollution Control, Nashville, TN 37206, USA

Correspondence to: Ellery Ingall (ingall@eas.gatech.edu)

Table S1 Summary of ambient PM2.5 collection

Location	Description	Date	No. of Individual Particles Examined
Fire Station 8	Urban	8.6.09	-
		8.26.09	-
		6.14.11	-
		6.17.11	-
		8.2.11	-
		8.11.11	5
		8.24.11	-
South DeKalb	Urban	8.5.09	-
		8.19.11	-
		8.24.11	4
		2.4.13	-
Jefferson Street	Urban Background	5.24.12	2
		8.6.12	-
Fort Yargo	Rural	9.17.08	5
		5.12.09	-
		6.10.11	5
		6.13.11	-
		8.18.11	-
Yorkville	Rural Background	6.20.12	2
		6.22.12	-
		6.29.12	-

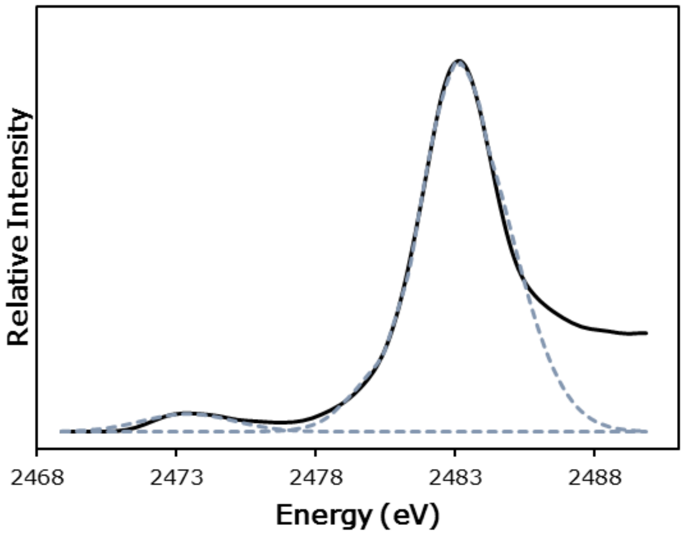

Figure S1: Gaussian peak fitting was used to determine the relative abundance of the S^0 and S^{+VI} oxidation state in the aerosol samples. Athena's peak fitting protocol was used to fit Gaussian curves (dotted line) to the S-NEXFS spectrum (solid line) and to determine the area under the Gaussian curves.

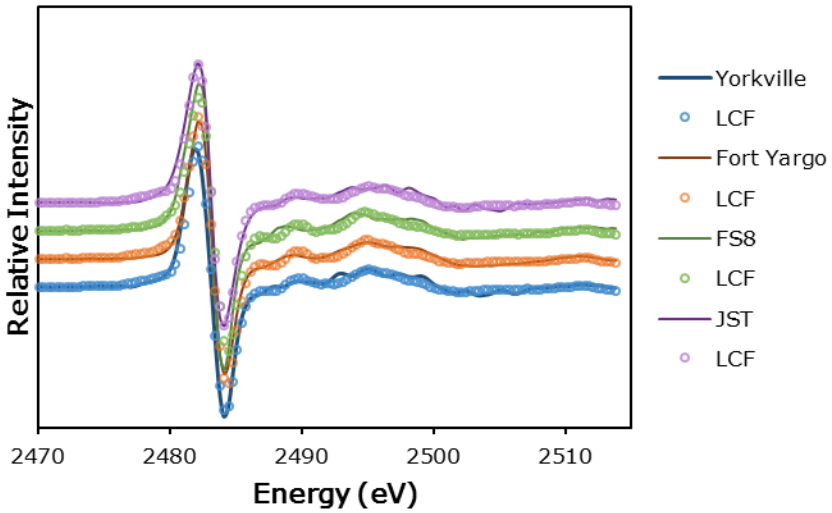

Figure S2: Linear combination fits of representative bulk samples. The first derivative was used to fit ambient aerosol samples (solid lines) with a database of sulfate standards. The resulting linear combination fits are shown with open circles.

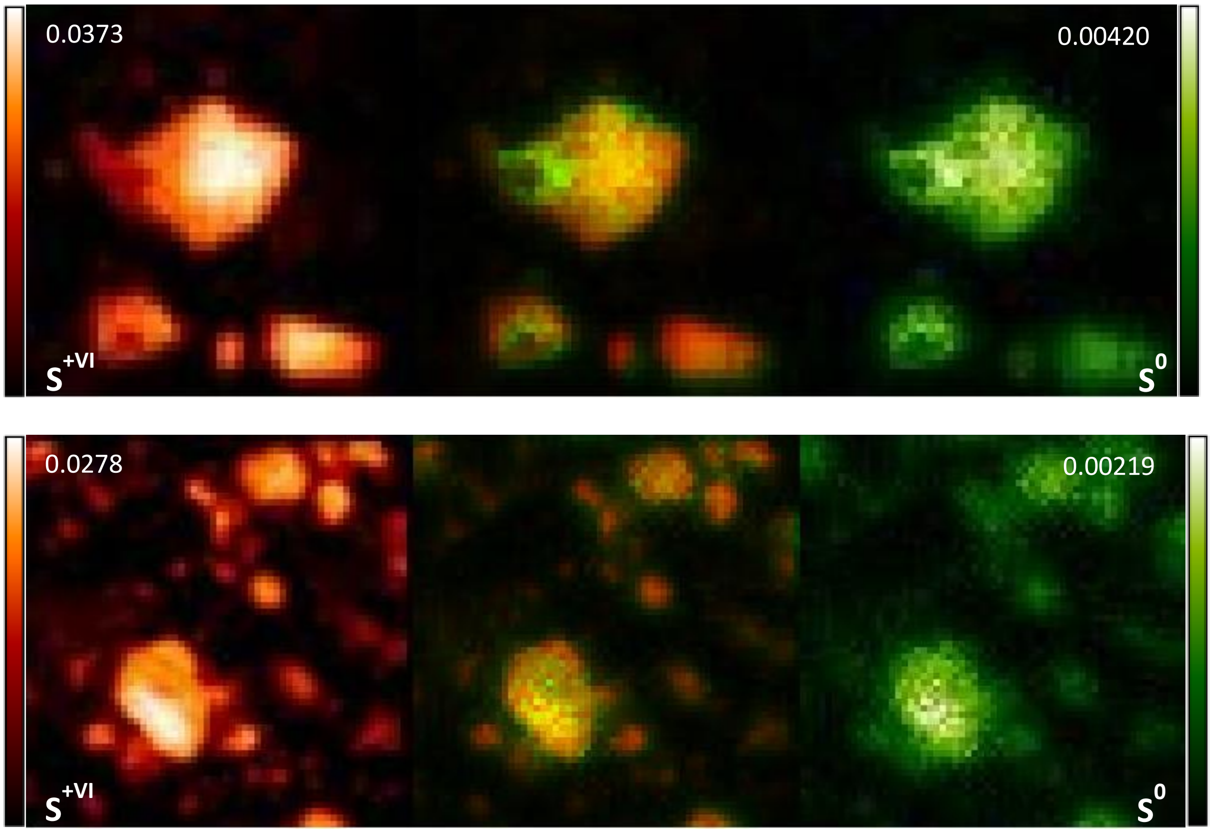

Figure S~~1~~3: X-ray fluorescence map of sulfur for two ambient particulate matter samples. The sulfur elemental density maps are scaled from black, lowest intensity, to white for the highest intensity. The maximum intensity value (in raw detector counts) for the elemental map is shown in the upper corner, with corresponding scale bars on the side of the elemental density maps. For both samples, S^{+VI} (red) is concentrated in the center of the particle, where the particle mass is highest. S^0 (green) has a more varied spatial distribution, but is generally concentrated in one specific area. An overlay of the S^0 and S^{+VI} elemental density is shown in the center.

Table S2 Composition of Sulfate from Bulk Ambient Aerosols and Emission Sources

Sampling Location	**Ammonium Sulfate**		**Cu(II) Sulfate**		**Gypsum**		**Iron(III) Sulfate**		**Potassium Sulfate**		***R* factor**
	%	±	%	±	%	±	%	±	%	±	
Yorkville	61.3	8.5	-	-	-	-	38.7	8.5	-	-	0.096963
Fort Yargo	83.9	7.4	-	-	-	-	16.1	7.4	-	-	0.0767302
Fire Station 8	86.5	6.5	13.5	16.3	-	-	-	-	-	-	0.0692747
Jefferson St	50.5	7.5	-	-	-	-	49.5	10.4	-	-	0.06186
South Dekalb 8/11	62.9	6.7	-	-	-	-	28.8	6.3	8.3	12.7	0.0169871
South Dekalb 2/13	42.3	13.9	-	-	-	-	57.7	13.9	-	-	0.0792618
South Dekalb 8/09	-	-	-	-	42.5	14.5	57.5	14.5	-	-	0.2040939
Biomass Burning	-	-	-	-	-	-	-	-	100.0	0.0	0.3686555
CFA	-	-	-	-	100.0	0.0	-	-	-	-	0.1054832
Diesel	70.2	11.0	-	-	-	-	29.8	12.4	-	-	0.034851

Table S3 Composition of Sulfate in Individual Particles

Sample ID	Ammonium Sulfate		Cu(II) Sulfate		Gypsum		Iron(III) Sulfate		Potassium Sulfate		Jarosite		*R* factor
	%	±	%	±	%	±	%	±	%	±	%	±	
FS8 8.11.11 P1	52.7	6.5	47.3	5.0	-	-	-	-	-	-	-	-	0.07684
FS8 8.11.11 P2	100.0	0.0	-	-	-	-	0.0	13.8	-	-	-	-	0.84504
FS8 8.11.11 P3	14.1	11.6	56.6	16.9	29.3	8.3	-	-	-	-	-	-	0.1339
FS8 8.11.11 P4	57.6	11.9	-	-	28.5	14.5	-	-	-	-	13.9	23.0	0.12948
FY 6.10.11 P1	59.1	10.0	-	-	32.2	7.6	-	-	8.6	5.0	-	-	0.035425
FY 6.10.11 P2	37.3	6.4	62.7	4.7	-	-	-	-	-	-	-	-	0.081002
FY 6.10.11 P3	-	-	100.0	0.0	-	-	-	-	-	-	-	-	0.11171
FY 6.10.11 P4	67.6	5.9	-	-	-	-	-	-	32.4	5.9	-	-	0.10811
FY 9.17.08 P1	29.5	16.6	70.5	3.6	-	-	-	-	-	-	-	-	0.53495
FY 9.17.08 P2	70.0	3.4	-	-	-	-	-	-	30.0	6.8	-	-	0.038327
FY 9.17.08 P3	65.5	7.9	-	-	-	-	-	-	34.5	5.1	-	-	0.080905
FY 9.17.08 P4	65.3	5.6	-	-	-	-	-	-	34.7	9.3	-	-	0.0143
FY 9.17.08 P5	80.1	8.9	-	-	-	-	-	-	19.9	31.0	-	-	0.17596
SD 8.24.11 P1	-	-	64.2	3.1	-	-	35.8	17.3	-	-	-	-	0.42401
SD 8.24.11 P2	100.0	0.0	-	-	-	-	-	-	-	-	-	-	0.49603
SD 8.24.11 P3	-	-	-	-	-	-	100.0	16.0	-	-	-	-	0.09181
SD 8.24.11 P4	100.0	19.4	-	-	-	-	-	-	-	-	-	-	0.67987